Thermolubricity of gas monolayers on graphene

Pierno, Matteo; Bignardi, Luca; Righi, Maria Clelia ; Bruschi, Lorenzo; Gottardi, Stefano; Stöhr, Meike; Ivashenko, Oleksii; Silvestrelli, Pierluigi; Rudolf, Petra; Mistura, Giampaolo

Published in:
Nanoscale

DOI:
10.1039/c4nr01079e

Publication date:
2014

Nanoscale

Accepted Manuscript

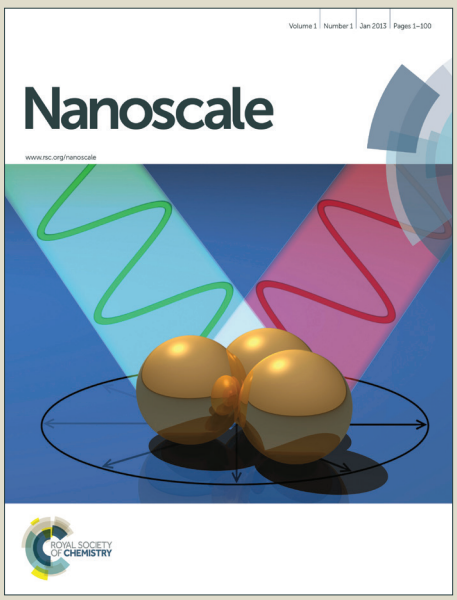

ROYAL SOCIETY OF CHEMISTRY

www.rsc.org/nanoscale

ARTICLE TYPE www. rsc.org/xxxxxx | XXXXXXXX

Thermolubricity of gas monolayers on graphene

View Article Online
DOI: 10.1039/C4NR01079E

Matteo Pierno,[a] Luca Bignardi,[†b] Maria Clelia Righi,[*c] Lorenzo Bruschi,[a] Stefano Gottardi,[b] Meike Stöhr, [b] Oleksii Ivashenko, [‡ b] Pier Luigi Silvestrelli, [a,d] Petra Rudolf [*b] and Giampaolo Mistura [*a]

Received Xth XXXXXXXXXX 20XX, Accepted Xth XXXXXXXXX 20XX
First published on the web Xth XXXXXXXXXX 200X
DOI: 10.1039/b000000x

Nanofriction of Xe, Kr and N_2 monolayers deposited on graphene was explored with a quartz crystal microbalance (QCM) at temperatures between 25 and 50 K. Graphene was grown by chemical vapour deposition and transferred to the QCM electrodes with a polymer stamp. Graphene was found to strongly adhere to the gold electrodes at temperatures as low as 5 K and at frequencies up to 5 MHz. At low temperatures, the Xe monolayers are fully pinned to the graphene surface. Above 30 K, the Xe film slides and the depinning onset coverage beyond which the film starts sliding decreases with temperature. Similar measurements repeated on bare gold show an enhanced slippage of the Xe films and a decrease of the depinning temperature below 25 K. Nanofriction measurements of Kr and N_2 confirm this scenario. This thermolubric behaviour is explained in terms of a recent theory of the size dependence of static friction between adsorbed islands and crystalline substrates.

1 Introduction

Since its discovery, graphene has been found to possess numerous outstanding properties such as extreme mechanical strength, extraordinarily high electronic and thermal conductivity, thus opening the way to a plethora of possible applications[1]. In particular, the tribological features of graphene have received increasing attention in view of the development of graphene-based coatings[2]. Graphite is a well-known solid lubricant, used in many practical applications. Its nanofriction behaviour has been investigated mainly by frictional force microscopy[3–5]. Measurements on few-layer graphene and single-layer graphene, prepared by micromechanical cleaving on weakly adherent substrates, have revealed that friction monotonically increases as the number of layers decreases[2,6,7], while, surprisingly, recent studies showed that this tendency is inverted when graphene is suspended[8].

The quartz crystal microbalance technique (QCM) is a powerful probe of interfacial phenomena that has been successfully employed to investigate the sliding friction of objects of nanoscopic size subject to lateral speeds as large as a few m/s[3]. Here we present the results of a QCM study mainly focused on the sliding of Xe, Kr and N_2 monolayers on graphene between 20 and 50 K, a temperature range which has been scarcely investigated in the literature[9], despite its relevance for the formation of condensed two-dimensional phases of many simple gases[10,11]. Monolayer Xe on graphite displays the phase diagram expected for a two-dimensional system that is only slightly perturbed by the corrugation of the surface potential[12]. It features a classical triple point at a temperature of 99 K where three different phases coexist: incommensurate solid, liquid and gas, which are the analogue of the bulk phases. Instead, the monolayer phase diagram of N_2 on graphite[13] lacks a similar triple point as does Kr on graphite[14]. The low temperature behaviour of these two systems is dominated by a solid phase commensurate to the graphite surface.

In our approach, the gold electrodes of a QCM were covered with graphene because the ample availability of phase diagrams of noble gases monolayers adsorbed on graphite[10] facilitates the interpretation of the QCM sliding measurements[15,16]. The QCM measurements of the sliding of Xe, Kr and N_2 monolayers on graphene provide the first evidence of thermal lubricity of adsorbed films.

2 Experimental

The microbalance used in our study consists of a small quartz disk (diameter 1 cm, thickness 1 mm) with the principal faces optically polished and covered by gold films, which are used both as electrodes and as adsorption surfaces. At the resonance frequency of 5 MHz, the two parallel faces of the QCM oscillate in a transverse shear motion. The condensation of

[a] *Dipartimento di Fisica e Astronomia 'G. Galilei' Università di Padova and CNISM, Via Marzolo, 8 I-35131 Padova, Italy*
[b] *Zernike Institute for Advanced Materials, University of Groningen, Nijenborgh 4, 9747AG Groningen, The Netherlands.*
[†] *Current address: Physikalisches Institut, Westfälische Wilhlems-Universität, 48149 Münster, Germany.*
[‡] *Current address: National Institute for Nanotechnology, University of Alberta 11421, Saskatchewan Dr., T6G 2M9 Edmonton AB, Canada.*
[c] *Istituto Nanoscienze, CNR and Department of Physics, Informatics and Mathematics, Università di Modena e Reggio, 41125 Modena, Italy.*
[d] *DEMOCRITOS National Simulation Center, of the Italian Istituto Officina dei Materiali (IOM) of the Italian National Research Council (CNR), Trieste, Italy.*

a film on the electrodes is signalled by a decrease in the resonance frequency. Any dissipation taking place at the solid-film interface is instead detected by a decrease in the corresponding resonance amplitude.

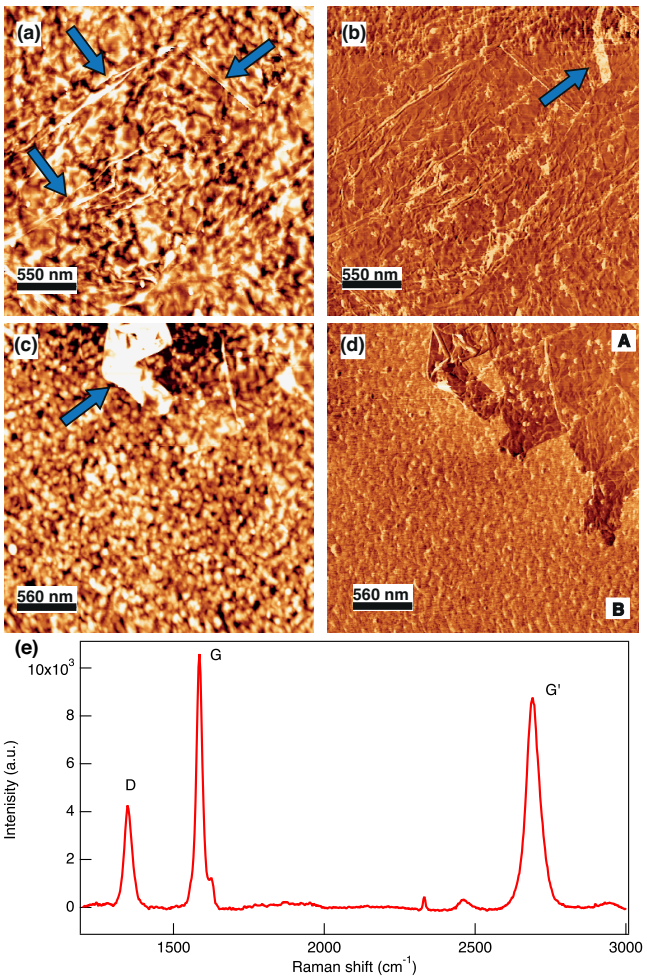

Fig. 1 (Colour online) Topography (a) and lateral force (b) micrographs of the graphene-coated quartz electrode obtained with an atomic force microscope. Brighter regions indicate higher height/friction. In the topography image wrinkles on the surface (blue arrows) are evidence of the presence of graphene. The lateral force micrograph shows homogeneous friction all over the surface, except at wrinkles and holes in the graphene (blue arrow). Topography (c) and lateral friction (d) micrographs of an area only partially covered by graphene close to the edge of the gold electrode. The observed features and roughness are comparable to those in panel (a). An area where the graphene is folded is indicated by the arrow. In the lateral friction micrograph (d) region *A* is covered by graphene while in region *B* the Au surface is bare. **(e)** Raman spectrum of CVD graphene transferred on SiO×(300 nm)/Si wafer. The relevant Raman peaks for graphene are labelled. The features at about 2330 and 2450 cm^{-1} are artefacts from the detector.

In previous QCM experiments graphene was grown epitaxially in-situ on a Ni(111) QCM electrode by heating the QCM to 400 °C in presence of carbon monoxide[17,18]. However, no direct morphological characterization of the resulting graphene coating was reported. In our experiment, graphene was grown ex-situ, transferred to the gold QCM electrode with a polymer stamp and fully characterized with a variety of microscopies. Graphene was grown by chemical vapor deposition (CVD) on an ultra-pure copper foil (purity 99.999%, ESPI metals) in a quartz-tube vacuum furnace (base pressure 10^{-5} mbar). The Cu foil was prepared with a preliminary etching in a 0.25 M solution of H_2SO_4 for 5 min and then rinsed in water. The substrates were then inserted in the furnace and reduced in H_2 (0.5 mbar) and Ar (0.1 mbar) for 60 min at 1180 K. Subsequently graphene was grown by exposing the Cu foil to Ar (0.1 mbar), H_2 (0.5 mbar) and methane (0.5 mbar) for 2 min at the same temperature[19]. After graphene growth, the samples were cooled down to room temperature in an Ar flux. Graphene was then transferred onto a polydimethylsiloxane (PDMS) stamp and the copper was etched away with an aqueous solution of $FeCl_3$. After rinsing with milliQ water and drying in a N_2 flow, the graphene layer was transferred from the PDMS stamp onto the Au electrode of the quartz crystal by applying pressure and peeling the stamp off.

The graphene layer on the Au electrode was characterized by contact-mode atomic force microscopy (AFM) using a Scientec 5100 instrument equipped with a silicon nitride cantilever on which a tip with a nominal radius <10 nm (force constant of 25-75 Nm^{-1}) was mounted. The image analysis was performed with the WSxM software[20]. The transferred graphene covered approximately $90 \pm 5\%$ of the electrode surface, as determined by a combination of AFM and optical microscopy. Figure 1-(a) shows a topography AFM micrograph ($3 \times 3\ \mu m^2$) of a graphene-coated area where wrinkles in the graphene layer are clearly visible (blue arrows); the root mean square (RMS) roughness measured on such an area was 3.4 nm. Surface diffraction experiments carried out on layers prepared in the same fashion yield sizes of single-crystalline grains ranging from 100 nm up to 5 μm[21]. Figure 1-(b) presents a lateral force microscopy (LFM) scan of the same area shown in Fig. 1-(a), which appears homogeneous, except along the wrinkles, where the lateral friction is higher. A hole in the graphene membrane (blue arrow) appears as an area with higher friction. Figure 1-(c) shows a topography AFM micrograph of an area at the electrode edge only partially covered by graphene. The roughness of this area is uniform, revealing no differences in topography between covered and uncovered areas, thus suggesting that graphene adheres to all asperities of the Au electrode. The RMS roughness measured on bare Au is 2.6 nm. Finally, Fig. 1-(d) shows the LFM scan of the same area where two regions with different friction are identified: the low-friction region A corresponds to

the graphene coating, the high-friction region B to bare Au, as explained in earlier friction experiments on graphene[6].

Raman spectroscopy was carried out by an Olympus BX51 microscope fiber-coupled to an Andor-Technology BV420A-DV detector and to a 532 nm laser (25 mW, Cobolt Technology)[21]. The laser spot size at the sample was ca. 10 μm with a 50$\times$ objective. The spectra were acquired on graphene prepared according to the procedure previously described but transferred on a SiO_2 (300 nm)/Si wafer to enhance the detection of the graphene-related peaks. However, this measurement provides a survey on the defects amount produced by the transfer process itself. In figure 1-(e) we report a typical Raman spectrum. As for any graphitic material, the high frequency E_{2gn} Raman allowed optical phonon mode, known as G peak (1590 cm^{-1}) and the G' (2690 cm^{-1}) band[22] due to a two-phonon double resonance Raman scattering process, feature prominently in the spectrum. The G' band could be fitted with a single Lorentzian peak (FWHM= 52 cm^{-1}). Similar spectra were measured on 3-4 spots located randomly on the sample indicating that $95 \pm 5\%$ of the transferred graphene is single layer[23]. Moreover, a relevant D band ($1370 - 1400$ cm^{-1}) was observed, which assigned to an A_{1g} breathing mode activated by the relaxation of the Raman selection rule in the presence of defects and therefore indicates that defects are present in the layer. By following the approach proposed by Lucchese *et al.*[24] the average distance between two point defects (L_D) in the layer can be estimated from the ratio of the intensities of the G and D peaks. We found that the ratio $I_D/I_G \simeq 0.3$, which corresponds to an average distance L_D of ca. 20 nm.

Identically prepared graphene-coated quartz crystals were inserted in a custom made mounting and annealed to about 200°C overnight in an UHV chamber housing the cold head of a 4 K cryocooler[25]. The quality factor Q in vacuum and at low temperature of the various quartz plated crystals tested in this study, ranged between 50000 and 140000, indicating a very good adhesion between graphene and gold. The measurements discussed in the next section were taken with the quartz having the highest Q factor, similar to the values of quartz plates with bare gold electrodes. As a comparison, the low temperature Q factor of the QCM with Pb electrodes evapourated onto quartz blanks was 90000[26].

Stainless steel spacers thermally decoupled the QCM holder from the cold head. The adsorbate layer was condensed directly onto the QCM, kept at the chosen low temperature, by slowly leaking high-purity gas through a nozzle facing the quartz electrode. Between consecutive deposition scans, the QCM was warmed up to about 60 K to guarantee full evapouration of Xe and thermal annealing of the microbalance[27]. The slip time, τ_s, describing the viscous coupling between substrate and film, can be calculated from the shifts in the resonance frequency and amplitude of the QCM[28]. τ_s represents the time constant of the exponential film velocity decay when the oscillating substrate is brought to a sudden stop. A low τ_s indicates high interfacial viscosity; if a film is rigidly locked to the substrate, τ_s goes to zero.

3 Results and discussion

Figure 2-(a) shows the slip time of Xe films deposited on graphene at different temperatures, T, and for coverages, Θ up to one monolayer (ML). The coverage was deduced from the frequency shift assuming for the ML an areal density of 5.94 atoms/nm^2, which corresponds to the completion of a solid incommensurate phase on the graphite lattice with nearest-neighbour distance $L_{nn} = 0.441$ nm[10,17]. This implies a frequency shift for this ML of about 7.6 Hz. For each T the average of a few runs or the most representative scan is reported for the sake of clarity. Data for $\Theta \leq 0.1$ ML are not plotted because of their intrinsically large fluctuations.

At $T < 30$ K, τ_s is practically zero, indicating that the Xe film is completely pinned to graphene. These findings are consistent with previous studies at low T reporting complete pinning of the highly polarizable N_2, Ar, Kr and Xe and sliding of the weakly polarizable Ne, ^{4}He and ^{3}He on different surfaces[26,29–33]. At $T = 35$ K, the film is pinned to the surface when the Xe coverage is very low but starts to slide for $\Theta > 0.45$ ML. As the temperature is further increased, τ_s increases monotonically while the depinning onset coverage, Θ_{dep}, beyond which the film starts to slide, decreases progressively. At the maximum temperature that could be achieved, $T = 46$ K, the slip time at monolayer completion is ≈ 0.5 ns , much smaller than the value of ≈ 1.7 ns measured at 77 K[17]. This behaviour clearly suggests that the sliding of the Xe film is favoured by temperature. Similar thermolubric effects have been reported for the friction of a tip moving along a graphite surface[34] and calculated in various models[35].

The slippage of Xe/graphene is significantly different from what is observed on bare Au electrodes. As shown in Fig. 2-(b), the Xe slip times measured on Au are much higher than those on graphene and Θ_{dep} is low even at $T = 25$ K. This difference is more evident in Fig. 3, which reports the temperature dependence of Θ_{dep} for all systems. The error bars refer to the standard deviation of data taken in different measurement runs. The vertical dashed line indicates the temperature below which the Xe monolayer is pinned to graphene. These data are indicative of a thermal depinning transition with a characteristic temperature, T_{dep} comprised between 30 and 35 K for Xe/graphene and below 25 K for Xe/Au.

As reported in Fig. 3, a similar thermal depinning was also observed for Kr and N_2 films, the only difference being that

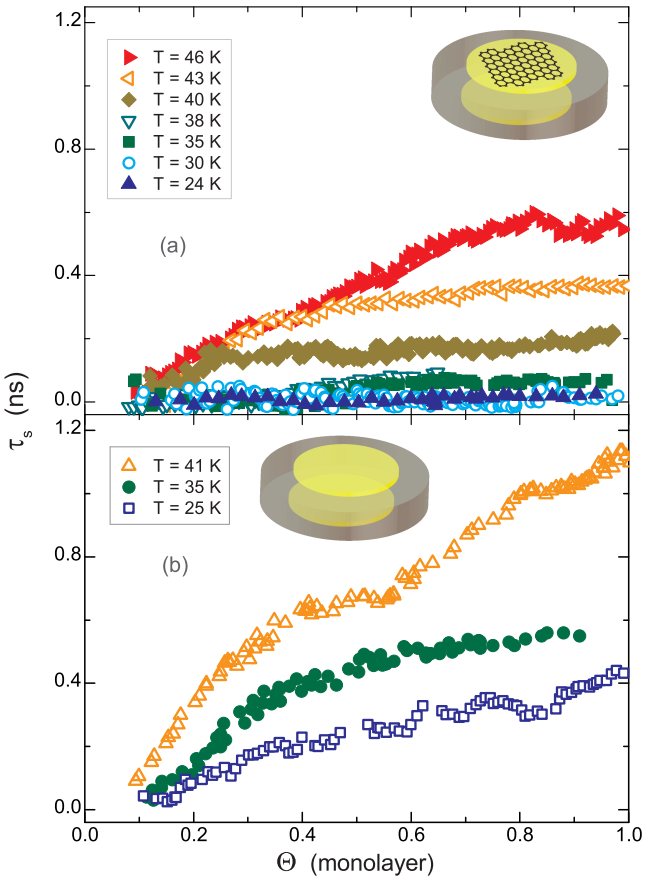

Fig. 2 (Colour online) Slip time as a function of Xe coverage at different temperatures for (a) Xe on graphene and (b) Xe on gold.

the characteristic temperatures are shifted to lower values reflecting the smaller polarizability of these adsorbates as compared to Xe. For Kr/graphene, the monolayer is fully pinned at 20 K so that $\Theta_{dep} \approx 22$ K while, in the case of N_2, Θ_{dep} cannot be identified due to the narrow temperature range accessible in our experiments. In fact, the data acquisition is limited below to about 20 K, by the thermal coupling of the QCM to the head of the cryocooler and above to 24 K by the evapouration of N_2 at $\Theta_{dep} \approx 1$. This implies that T_{dep} must be lower than 20 K for both surfaces. Interestingly, in the explored temperature domain we have not seen any evidence of pinning due to the formation of a solid phase commensurate to the surface[13,14]. This may suggest that the commensurate phase found on graphite disappears for solid Kr and N_2 monolayers deposited on a graphene/gold surface. Another possibility is that the driving amplitude of the quartz crystal is enough to depin the solid monolayer[36].

Neglecting the contributions due to the surface roughness and the finite size of the crystalline domains , whose effects are quite difficult to evaluate, one possible explanation of the observed difference between graphene and Au surfaces is the higher corrugation of the surface potential on graphene with respect to gold. Recent QCM experiments of Xe on a variety of metallic electrodes have verified that the measured slip time is inversely proportional to U_0^2, where U_0 is the amplitude of the periodic function describing the changes in adsorbate-substrate potential with respect to adsorbate position[17]. For Xe/graphene, U_0 amounts to 5.3 meV[17] while there is no U_0 value reported in the literature for Xe/Au. We have estimated the corrugation amplitude U_0 for Xe on Au and graphene using an *ab-initio* scheme based on the recently-developed nonlocal rVV10 density functionals[37] (including an accurate description of van der Waals effects implemented in the QE package[38]).

View Article Online
DOI: 10.1039/C4NR01079E

The interaction of a Xe atom and of a N_2 molecule with both the ideal, planar single layer of graphene and the Au(111) surface were considered. The computed U_0 value for Xe/graphene, 2.2 meV, is significantly larger than that for Xe/Au (1.6 meV), thus supporting the explanation of the τ_s data based on the higher corrugation of the surface potential on graphene. It is worthwhile to point out that, although the absolute values of the *ab-initio* estimates of the corrugation could significantly depend on technical details such as the chosen density functional, their ratios are expected to be much less sensitive to such particulars and therefore much more reliable. Moreover the tabulated value of U_0 for Xe/graphene refers to graphene grown on Ni(111)[17], which could explain the discrepancy with our value computed for an ideal, isolated layer of graphene. For N_2 we instead find U_0 values of 8.0 and 6.6 meV for N_2/graphene and N_2/Au, respectively.

As for the observed temperature dependence of τ_s, this is partly consistent with dynamic simulations of the sliding of model Xe layers on weakly corrugated surfaces[35,39]. The major difference between our data and the aforementioned molecular simulations[39] is the occurrence of a depinning onset coverage which depends on temperature as clearly displayed in Fig. 3 and which contrasts with the sliding at low Θ observed in the simulations.

An interpretation of the observed decrease of Θ_{dep} with temperature relies on a recent theory[40] about the size dependence of static friction between adsorbed islands and crystalline substrates according to which the atomic structure of islands deposited on a substrate of nonmatching lattice parameters consists of commensurate domains separated by incommensurate domain walls. Domain structures are governed by the competition in minimizing both interfacial energy and elastic strain energy. When the size of the contact is reduced below a critical radius, R_c, domains coalesce. This structural transition is accompanied by a sharp increase of the interfacial commensurability and static friction[40]. The depinning of a commensurate interface has been shown to be a thermally activated process with an associated barrier

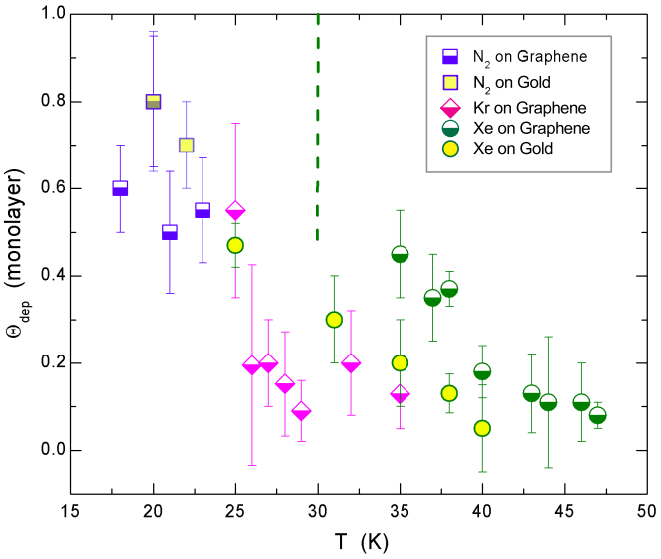

Fig. 3 (Colour online) Depinning onset coverage as a function of temperature for the systems investigated in this work. Dashed line indicates the temperature below which Xe monolayers are always pinned to graphene. Error bars account for data distributions over different runs performed at different thermal cool downs from room temperature and different surfaces. The number of averaged datapoints goes from a minimum of 3 to about a dozen. The largest error bars refer to the smallest ensembles.

$E_{\rm dep} \propto \varepsilon U_0(F_{\rm s}-F)/F_{\rm s}F$, where F is the applied lateral force and $F_{\rm s}$ the static friction force[41]. In the case of perfect commensurability, the huge difference between the static friction force and the weak inertia force provided by the oscillating QCM results in a very high activation barrier (for example, $E_{\rm dep} \simeq 10^7$ eV has been estimated for a Xe monolayer on the Cu(111) surface in the absence of defects). Such barrier has been found to drop dramatically by decreasing the interfacial commensurability[41]. By combining these results with the experimental findings, the following interpretation of the QCM data is proposed:

i) The observation of a *thermally activated frictional slip* in nominally incommensurate Xe/graphene and Xe/Au systems can be accounted for by the predicted increase of commensurability at small sizes. Islands of radius lower than R_c are expected to be pinned to the QCM but thermal depinning becomes probable at larger size due to the decrease of static friction, $F_{\rm s}$.

ii) The *critical coverage* necessary for the depinning of the film, $\Theta_{\rm dep}$, is related to the coverage necessary for the growing Xe islands to reach a large enough size, $R_{\rm dep} \geq R_c$, for the depinning process to be activated at the considered temperature. This seems confirmed by the fact that the critical size estimated for Xe on graphene is larger than that on Au in agreement with the experimental observation that $\Theta_{\rm dep}$ is larger for Xe/graphene than for Xe/Au (see Fig. 3). The major contribution to the calculated difference in the critical size comes from the different misfit strain e. R_c is, in fact proportional to $(1/e^2)$[40], where $e=-0.083$ for Xe/graphene and $e=0.13$ for Xe/Au.

Although this scenario is found to apply to Xe/graphene, its validity should be quite general.

Preliminary molecular dynamics simulations of Xe on graphene confirm that the adsorbate islands are commensurate at low coverage and the commensurability decreases both with the temperature and coverage increase

4 Conclusions

In summary, we have successfully managed to transfer graphene to the gold electrode of a QCM and the adhesion is found to be very good even at cryogenic temperatures (e.g. down to 10 K) and at oscillating frequencies of 5 MHz. The presence of graphene on the gold electrode significantly affects the sliding of Xe films. The measured slip time is about half that on bare gold, probably because of the higher corrugation of the surface potential on graphene with respect to gold. Overall, the solid films are found to be rigidly pinned to the surface at sufficiently low temperatures and start sliding at higher temperatures. The onset coverage for sliding decreases with temperature and at a given temperature is smaller on bare gold. Nanofriction measurements on Kr and N_2 confirm this thermal depinning This thermolubric behaviour is explained in terms of a recent theory of the size dependence of static friction between adsorbed islands and crystalline substrates. This study provides the first direct evidence of thermal lubricity of adsorbed films.

This work was supported by the "Graphene-based electronics" research program and a Projectruimte grant of the Stichting voor Fundamenteel Onderzoek der Materie (FOM), part of the Nederlandse Organisatie voor Wetenschappelijk Onderzoek (NWO). The authors thank Prof. Dr. W. R. Browne for allowing them to use the Raman microscope.

References

1 K. S. Novoselov, V. I. Falko, L. Colombo, P. R. Gellert, M. G. Schwab and K. Kim, *Nature*, 2012, **490**, 192–200.
2 C. Lee, Q. Li, W. Kalb, X.-Z. Liu, H. Berger, R. W. Carpick and J. Hone, *Science*, 2010, **328**, 76–80.
3 E. Gnecco and E. Meyer, *Fundamentals of Friction and Wear*, Springer, 2007.
4 M. Dienwiebel, G. S. Verhoeven, N. Pradeep, J. W. M. Frenken, J. A. Heimberg and H. W. Zandbergen, *Phys. Rev. Lett.*, 2004, **92**, 126101.

5 S. Koch, D. Stradi, E. Gnecco, S. Barja, S. Kawai, C. Díaz, M. Alcamí, F. Martín, A. L. Vázquez de Parga, R. Miranda, T. Glatzel and E. Meyer, *ACS Nano*, 2013, **7**, 2927–2934.

6 T. Filleter, J. L. McChesney, A. Bostwick, E. Rotenberg, K. V. Emtsev, T. Seyller, K. Horn and R. Bennewitz, *Phys. Rev. Lett.*, 2009, **102**, 086102.

7 T. Filleter and R. Bennewitz, *Phys. Rev. B*, 2010, **81**, 155412.

8 Z. Deng, N. N. Klimov, S. D. Solares, T. Li, H. Xu and R. J. Cannara, *Langmuir*, 2013, **29**, 235–243.

9 M. F. Danisman and B. Özkan, *Rev. Sci. Instrum.*, 2011, **82**, 115104–115104–7.

10 L. W. Bruch, R. D. Diehl and J. A. Venables, *Rev. Mod. Phys.*, 2007, **79**, 1381–1454.

11 L. Bruch, M. Cole and E. Zaremba, *Physical adsorption: forces and phenomena*, Clarendon Press, 1997.

12 A. Thomy, X. Duval and J. Regnier, *Surface Science Reports*, 1981, **1**, 1 – 38.

13 M. H. W. Chan, A. D. Migone, K. D. Miner and Z. R. Li, *Phys. Rev. B*, 1984, **30**, 2681–2694.

14 D. M. Butler, J. A. Litzinger, G. A. Stewart and R. B. Griffiths, *Phys. Rev. Lett.*, 1979, **42**, 1289–1292.

15 N. Hosomi, A. Tanabe, M. Suzuki and M. Hieda, *Phys. Rev. B*, 2007, **75**, 064513.

16 N. Hosomi, J. Taniguchi, M. Suzuki and T. Minoguchi, *Phys. Rev. B*, 2009, **79**, 172503.

17 T. Coffey and J. Krim, *Phys. Rev. Lett.*, 2005, **95**, 076101.

18 M. Walker, C. Jaye, J. Krim and M. W. Cole, *J. Phys.: Condens. Matter*, 2012, **24**, 424201.

19 C. Mattevi, H. Kim and M. Chhowalla, *J. Mater. Chem.*, 2011, **21**, 3324–3334.

20 I. Horcas, R. Fernández, J. M. Gómez-Rodríguez, J. Colchero, J. Gómez-Herrero and A. M. Baro, *Rev. Sci. Instrum.*, 2007, **78**, 013705–013705–8.

21 L. Bignardi, W. F. van Dorp, S. Gottardi, O. Ivashenko, P. Dudin, A. Barinov, J. T. M. De Hosson, M. Stohr and P. Rudolf, *Nanoscale*, 2013, **5**, 9057–9061.

22 L. G. Cançado, A. Jorio, E. M. Ferreira, F. Stavale, C. Achete, R. Capaz, M. Moutinho, A. Lombardo, T. Kulmala and A. Ferrari, *Nano letters*, 2011, **11**, 3190–3196.

23 J. Park, A. Reina, R. Saito, J. Kong, G. Dresselhaus and M. Dresselhaus, *Carbon*, 2009, **47**, 1303–1310.

24 M. M. Lucchese, F. Stavale, E. Ferreira, C. Vilani, M. Moutinho, R. B. Capaz, C. Achete and A. Jorio, *Carbon*, 2010, **48**, 1592–1597.

25 L. Bruschi, A. Carlin, F. Buatier de Mongeot, F. dalla Longa, L. Stringher and G. Mistura, *Rev. Sci. Instrum.*, 2005, **76**, 023904–023904–5.

26 M. Pierno, L. Bruschi, G. Fois, G. Mistura, C. Boragno, F. B. de Mongeot and U. Valbusa, *Phys. Rev. Lett.*, 2010, **105**, 016102.

27 M. Pierno, L. Bruschi, G. Mistura, C. Boragno, F. B. de Mongeot, U. Valbusa and C. Martella, *Phys. Rev. B*, 2011, **84**, 035448.

28 L. Bruschi and G. Mistura, *Phys. Rev. B*, 2001, **63**, 235411.

29 R. L. Renner, P. Taborek and J. E. Rutledge, *Phys. Rev. B*, 2001, **63**, 233405.

30 G. Fois, L. Bruschi, L. d'Apolito, G. Mistura, B. Torre, F. B. d. Mongeot, C. Boragno, R. Buzio and U. Valbusa, *J. Phys.: Condens. Matter*, 2007, **19**, 305013.

31 M. Highland and J. Krim, *Phys. Rev. Lett.*, 2006, **96**, 226107.

32 L. Bruschi, G. Fois, A. Pontarollo, G. Mistura, B. Torre, F. Buatier de Mongeot, C. Boragno, R. Buzio and U. Valbusa, *Phys. Rev. Lett.*, 2006, **96**, 216101.

33 T. Oda and M. Hieda, *Phys. Rev. Lett.*, 2013, **111**, 106101.

34 K. B. Jinesh, S. Y. Krylov, H. Valk, M. Dienwiebel and J. W. M. Frenken, *Phys. Rev. B*, 2008, **78**, 155440.

35 A. Vanossi, N. Manini, M. Urbakh, S. Zapperi and E. Tosatti, *Rev. Mod. Phys.*, 2013, **85**, 529–552.

36 L. Bruschi, A. Carlin and G. Mistura, *Phys. Rev. Lett.*, 2002, **88**, 046105.

37 R. Sabatini, T. Gorni and S. de Gironcoli, *Phys. Rev. B*, 2013, **87**, 041108(R).

38 *http://www.quantum-espresso.org*.

39 B. N. J. Persson, *Phys. Rev. B*, 1993, **48**, 18140–18158.

40 M. Reguzzoni and M. C. Righi, *Phys. Rev. B*, 2012, **85**, 201412.

41 M. Reguzzoni, M. Ferrario, S. Zapperi and M. C. Righi, *Proc. Nat. Acad. Sci.*, 2010, **107**, 1311–1316.